A mechanical model of the half-sarcomere which includes the contribution of titin

I. Pertici, M. Caremani, and M. Reconditi

ABSTRACT

The evidence, in both resting and active muscle, for the presence of an I-band spring element like titin that anchors the Z line to the end of the thick filament did not yet produce a proper theoretical treatment in a complete model of the half-sarcomere. The textbook model developed by A.F. Huxley and his collaborators in 1981, which provides that the half-sarcomere compliance is due to the contribution of the compliances of the thin and thick filaments and actin-attached myosin motors, predicts that at any sarcomere length the absence of attached motors results in an infinite half-sarcomere compliance, in contrast with the observations. Growing evidence for the presence of a titin-like I-band spring urges the 1981 model to be implemented to include the contribution of this element in the mechanical model of the half-sarcomere. The model described here represents a tool for the interpretation of measurements of half-sarcomere compliance at long sarcomere lengths and for investigations of the possible role of titin as the mechano-sensor in thick filament regulation.

INTRODUCTION

In the striated (skeletal and cardiac) muscle, the contractile proteins myosin and actin are organized respectively in well-ordered thick and thin filaments in the sarcomere, the ca 2 µm long structural unit of muscle in which bipolar arrays of myosin II motors emerging from the thick filaments overlap with the thin filaments originating from the Z line bounding the sarcomere. Force and shortening during muscle contraction are due to cyclical ATP-driven interactions of the globular portion (the head) of the motors with the nearby actin monomers in the thin filaments. In each half-sarcomere (hs), the myosin motors are mechanically coupled as parallel force generators via their attachment to the thick filament, constituting, together with the interdigitating thin filaments and the other cytoskeleton and regulatory proteins, the basic functional unit of muscle (Fig. 1). Stiffness measurements at the level of the half-sarcomere directly inform on the stiffness and the number of actin-attached motors (cross-bridges) under the condition that they are the only source of compliance in the half-sarcomere (1,2). In contrast to this idea, X-ray diffraction experiments indicated that thin and thick filaments under stress (3-7) extend by 0.23–0.26% for a force change equivalent to T_0, the maximal force developed in an isometric tetanic contraction. Under these conditions the contribution of actin-attached cross-bridges and myofilaments to half-sarcomere compliance (C_{hs}) can be defined, in the framework of the model developed by Ford and colleagues (8; FHS1981 hereafter), in which, assuming that the compliance of the array of cross-bridges is not smaller than the cumulative compliance of the actin and myosin filaments, C_{hs} can be calculated by the sum of the equivalent compliances of the three elements (see Methods). The simple useful formulation of this equation is:

$$C_{\mathrm{hs}} = C_{\mathrm{f}} + \frac{1}{k_{\mathrm{c}}\zeta} \qquad (1)$$

Where C_f is the equivalent filament compliance, k_c is the stiffness per unit length of the array of the cross-bridges and ζ is the length of overlap of thin filament with the cross-bridges array in each half-sarcomere.

More recently, hs stiffness measurements by means of fast length oscillations applied to single muscle fibers during the development of an isometric tetanus have shown that at low forces, when the number of attached motors is relatively low, a significant contribution to C_{hs} emerges from another elastic element the compliance of which, C_p, is functionally in parallel with that of the attached motors (9-11). The value of C_p was somewhat controversial depending on the protocols used to estimate it. When stiffness measurements were made at the level of a selected population of sarcomeres in an isometrically contracting single frog fibre at 4 °C (plateau force T_0 ~150 kPa), it resulted to be 200-300 nm/MPa (11,12), that is ~20 times larger than the compliance of the array of motors attached at T_0 (11.5 nm/MPa). Such a relatively large compliance of the parallel elasticity explains why its contribution emerges only at low forces when the stiffness of the motor array becomes comparable to that of the parallel element. To consider the contribution of this element to the C_{hs} requires only a slight modification of the FHS1981 model. Namely, C_{hs} can be interpreted as the series of the filament compliance, C_f, and the compliance resulting from the parallel arrangement of the force-generating cross-bridges and the new element:

$$C_{hs} = C_f + \frac{C_p}{1+C_p k_c \zeta} \qquad (2)$$

This element could be associated to the presence of links connecting the thin and thick filaments in the A-band, like either a fraction of weakly bound, no-force generating motors (10,12), or the thick filament accessory protein myosin-binding protein C (Fig 1), which has shown to undergo dynamic interactions with the thin filament (13-19). Alternatively, a similar role of parallel elasticity could be played by an I-band spring, like the gigantic protein titin that spans the whole half-sarcomere, connecting the Z line at the end of the sarcomere with the tip of the thick filament and running bound to the surface of the thick filament up to the M-line at the center of the sarcomere (Fig. 1; 20-24). Titin, as an I-band spring, is the only element able to transmit the stress to thick filament also in the resting sarcomere, when no motors are attached to actin, which explains the passive force developed by a resting sarcomere when it is stretched. In frog skeletal muscle, this happens for sarcomere length (SL) > 2.50 µm and reaches ca 0.7 T_0 for SL ~ 3.4 µm (25). In this respect it must be noted that the cord compliance that can be calculated from the passive force – SL relation is (0.45 µm/(0.7·150 kPa) =) 4300 nm/MPa per hs, ~20 times larger than C_p determined at full overlap (11,12) and even larger than that determined at SL > 2.5 µm (26). Such a large difference in the titin-like I band spring finds a molecular explanation in the *in vitro* mechanical studies that allowed the definition of the load dependent structural dynamics of titin (27). demonstrating that titin stiffness is modulated in time by the load-dependent equilibrium between folding-unfolding of its immunoglobulin (Ig) domains. This finding suggests that the role of titin as I-band spring in parallel to the array of motors can be much more relevant than that of an elastic element that adds its contribution of force in the extreme condition of a weak half-sarcomere which has undergone a large stretch (29-30). Rather titin may work as a dynamic spring that provides a substantial contribution of force to prevent a weak half-sarcomere to give during contraction.

If the contribution of the parallel elasticity to C_{hs} were due to either weakly bound motors or any other A-band inter-filament link, the stiffness of the active muscle should reduce at long SL with the reduction of filament overlap. A more complex behavior is expected in the case of a titin-like I-band spring, as in this case the stiffness of the spring may vary with the large changes in its length accompanying the changes in SL. In this respect it is worth to note that, using large stretches, Bagni

and co-workers (31) identified an elastic element in parallel with the cross-bridges, defined as a 'static stiffness', which rises abruptly upon activation independent of motor attachment and increases with the increase of sarcomere length up to 2.8 μm. Even if the large stretch is a somewhat less direct mean for estimating stiffness changes, as the attached motors are brought into a regime which may imply also detachment-attachment kinetics, the results are intriguing and suggestive of a role of titin in active contraction. A further support to this idea derives from the finding that in vitro titin stiffness increases in the presence of Ca^{2+} (32).

The evidence, in both resting and active muscle, for the presence of an I-band spring element like titin that anchors the Z line to the end of the thick filament, makes FHS 1981 model no longer valid, because it assumes that, at any SL, the absence of cross-bridges results in an infinite half sarcomere compliance. Here we implement the FHS1981 model to include the contribution of an I-band spring to the half sarcomere compliance. The model represents a tool for the interpretation of measurements of hs stiffness at increasing SL, which is important either in relation to the mechanism of stabilisation of SL against the consequence of sarcomere inhomogeneity in active force generation, or for investigations on the role of titin as mechano-sensor in thick filament regulation (33-35).

METHODS

In the FHS 1981 model, assuming that the compliance of the array of cross-bridges is not smaller than the cumulative compliance of the actin and myosin filaments, C_{hs} can be calculated by the sum of the equivalent compliances of the three elements:

$$C_{\mathrm{hs}} = c_{\mathrm{A}}(l_{\mathrm{A}} - \zeta) + c_{\mathrm{M}}(l_{\mathrm{M}} - \zeta) + \frac{c_{\mathrm{A}} c_{\mathrm{M}}}{c_{\mathrm{A}} + c_{\mathrm{M}}}\zeta + \frac{c_{\mathrm{A}+} c_{\mathrm{M}}}{2\mu}\left\{\coth\left(\frac{\mu\zeta}{2}\right) + \left(\frac{c_{\mathrm{A}} - c_{\mathrm{M}}}{c_{\mathrm{A}} + c_{\mathrm{M}}}\right)^2 \tanh\left(\frac{\mu\zeta}{2}\right)\right\} + C_{\mathrm{Z}} \quad (3)$$

Where c_A and c_M are the compliances per unit length of the thin and thick filaments respectively, k_c is the stiffness per unit length of the array of the cross-bridges, C_Z is the compliance of the Z line, l_A and l_M are the length of the thin and thick filament respectively, ζ is the length of overlap of thin and thick filaments in each half-sarcomere and μ $\left(= (k_{\mathrm{c}}(c_{\mathrm{A}} + c_{\mathrm{M}}))^{\frac{1}{2}}\right)$ is a parameters that increases as the cumulative compliance of the filaments increases relative to that of the motor array ($1/k_c$).

Provided that $\mu\zeta/2$ is not too large, Eq. 1 simplifies to:

$$C_{\mathrm{hs}} = c_{\mathrm{A}}\left(l_{\mathrm{A}} - \frac{2}{3}\zeta\right) + c_{\mathrm{M}}\left(l_{\mathrm{M}} - \frac{2}{3}\zeta\right) + \frac{1}{k_{\mathrm{c}}\zeta} + C_{\mathrm{Z}} \quad (4)$$

Given the small axial extension of the Z line (~30–50 nm in the fast skeletal muscles; 36), its contribution C_Z to C_{hs} will be neglected hereafter. Estimates of c_A, c_M and k_c obtained from both X-ray diffraction and mechanical measurements (3-7,11,37) indicate that the condition $\mu\zeta/2 < 1$ is fulfilled. Consequently, according to the model, C_{hs} can be considered functionally as the series of two compliances: the myofilament compliance, $C_{\mathrm{f}} = c_{\mathrm{A}}\left(l_{\mathrm{A}} - \frac{2}{3}\zeta\right) + c_{\mathrm{M}}\left(l_{\mathrm{M}} - \frac{2}{3}\zeta\right)$ and the motor compliance, $1/k_{\mathrm{c}}\zeta$.

According to the model of FHS1981 (Fig. 2), an external force T applied to the hs is entirely born by the thick and thin filaments in the regions that do not overlap and is shared between the two filaments in the overlap region, where the cross-bridges transfer force between the two filaments. At any axial position the force born by the thin filament, T_A, and that born by the thick filament, T_M, add to give the total force T applied to the hs. Taking ξ as the axial distance measured from the

center of the overlap zone, and positive toward the Z line, the difference $dT_A(\xi) = T_A(\xi + d\xi) - T_A(\xi)$ in the force born by the thin filament along a small axial distance $d\xi$ at the coordinate ξ is $k_c\, d\xi\, x(\xi)$, where $k_c\, d\xi$ is the stiffness of the small cross-bridge segment $d\xi$ and $x(\xi)$ is the distortion of the cross-bridge array at that coordinate, taken positive for stretches (Fig. 3, upper panel). In the same way, for the thick filament $dT_M(\xi) = -k_c d\xi x(\xi)$, consistent with the fact that force is transferred between the two filaments through the cross-bridge array and, in each point along the hs, is the same and shared between the filaments in the overlap region. This leads to Eq. A1 of FHS1981:

$$\frac{dT_A}{d\xi} = -\frac{dT_M}{d\xi} = k_c x(\xi) \tag{5}$$

Over a small axial distance $d\xi$, the distortion of the cross-bridges differs by a quantity $dx(\xi) = x(\xi + d\xi) - x(\xi)$ that results from the different strain in the thin and thick filaments (Fig. 3, lower panel), so that:

$$dx(\xi) = T_A(\xi)\, c_A d\xi - T_M(\xi)\, c_M d\xi \tag{6}$$

and thus:

$$dx/d\xi = T_A(\xi) c_A - T_M(\xi) c_M = (c_A + c_M) T_A(\xi) - c_M T \tag{7}$$

that is Eq. A2 of FHS1981.

Differentiating (7) and substituting for $dT_A/d\xi$ from Eq. 5 gives

$$d^2x/d\xi^2 = k_c(c_A + c_M) x(\xi) \tag{8}$$

whose solution (Eq. A4a of FHS81) is

$$x(\xi) = x_0 \cosh\left(\mu\left(\xi - \xi_0\right)\right) \tag{9a}$$

where

$$\mu = (k_c(c_A + c_M))^{1/2} \tag{9b}$$

The presence of an elastic link between the end of the thick filament and the Z line, which is the role played by titin in the I band, changes the boundary conditions with respect to FHS1981 model, and in turns affects the expressions for x_0 and ξ_0. In the original model, at point A (Fig. 2) $\xi = -\frac{\zeta}{2}$ and $T_A\left(-\frac{\zeta}{2}\right) = 0$ and at point B $\xi = +\frac{\zeta}{2}$ and $T_M\left(+\frac{\zeta}{2}\right) = 0$.

In the presence of titin link, the force on the thick filament at B, i.e. at the end of the filament, is the same as that, T_T, born by titin in the I band. This force, added to T_A in the I band, gives the full force T found at the Z line:

$$T_T + T_A = T \tag{10}$$

Thus, to determine the boundary condition at *B*, one must first determine how T is distributed between thin filament and titin in the I band. To do that, we consider that under a force T on the hs, in the I band the strain of titin, $c_T(l_A - \zeta)T_T$, where c_T indicates the compliance of titin per unit length, must be the same as the strain of the thin filament, $c_A(l_A - \zeta)T_A$, plus the strain of the cross-bridges at *B*, x_B (Fig. 4):

$$c_T(l_A - \zeta)T_T = c_A(l_A - \zeta)T_A + x_B \tag{11}$$

Eq. 10 and Eq. 11 provide the expression for T_{A} and T_{T} in the I band (and thus their values in B) as:

$$T_{\mathrm{A}} = \frac{c_{\mathrm{T}}}{c_{\mathrm{A}}+c_{\mathrm{T}}}\left\{T - \frac{x_{\mathrm{B}}}{c_{\mathrm{T}}(l_{\mathrm{A}}-\zeta)}\right\} \tag{12}$$

$$T_{\mathrm{T}} = T - T_{\mathrm{A}} = \frac{c_{\mathrm{A}}}{c_{\mathrm{A}}+c_{\mathrm{T}}}\left\{T + \frac{x_{\mathrm{B}}}{c_{\mathrm{A}}(l_{\mathrm{A}}-\zeta)}\right\} \tag{13}$$

With this, the boundary conditions in A and B become respectively:

$$-c_{\mathrm{M}}T = \left(\frac{\mathrm{d}x}{\mathrm{d}\xi}\right)_{\mathrm{A}} = \mu x_0 \sinh\left(\mu\left(-\frac{\zeta}{2} - \xi_0\right)\right) \tag{14}$$

and

$$+c_{\mathrm{A}}T_{\mathrm{A}} - c_{\mathrm{M}}T_{\mathrm{T}} = \left(\frac{\mathrm{d}x}{\mathrm{d}\xi}\right)_{\mathrm{B}} = \mu x_0 \sinh\left(\mu\left(+\frac{\zeta}{2} - \xi_0\right)\right) \tag{15}$$

By using Eq. 11 and Eq. 12, Eq. 15 can be rearranged to:

$$+c_A \cdot T = \frac{\left(\frac{\mathrm{d}x}{\mathrm{d}\xi}\right)_B (c_{\mathrm{A}}+c_{\mathrm{T}})(l_{\mathrm{A}}-\zeta)+x_{\mathrm{B}}(c_{\mathrm{A}}+c_{\mathrm{M}})}{(c_{\mathrm{T}}-c_{\mathrm{M}})(l_{\mathrm{A}}-\zeta)} = x_0 \frac{\mu \sinh\left(\mu\left(+\frac{\zeta}{2}-\xi_0\right)\right)(c_{\mathrm{A}}+c_{\mathrm{T}})(l_{\mathrm{A}}-\zeta)+\cosh\left(\mu\left(+\frac{\zeta}{2}-\xi_0\right)\right)(c_{\mathrm{A}}+c_{\mathrm{M}})}{(c_{\mathrm{T}}-c_{\mathrm{M}})(l_{\mathrm{A}}-\zeta)} \tag{16}$$

Eq. 14 and Eq. 16 are then equivalent to Eq. A5a and Eq. A5b of FHS1981 respectively.

Equating Eq. 14 and Eq. 16 for T leads to:

$$\tanh(\mu\xi_0) = \frac{c_{\mathrm{M}}(c_{\mathrm{A}}+c_{\mathrm{M}})+\mu(l_{\mathrm{A}}-\zeta)[c_{\mathrm{T}}(c_{\mathrm{M}}-c_{\mathrm{A}})+2c_{\mathrm{M}}c_{\mathrm{A}}]\tanh\left(\mu\frac{\zeta}{2}\right)}{\mu(l_{\mathrm{A}}-\zeta)c_{\mathrm{T}}(c_{\mathrm{A}}+c_{\mathrm{M}})+c_{\mathrm{M}}(c_{\mathrm{A}}+c_{\mathrm{M}})\tanh\left(\mu\frac{\zeta}{2}\right)} \tag{17}$$

Subtracting Eq. 14 from Eq. 16 gives:

$$x_0 = \frac{(c_{\mathrm{T}}-c_{\mathrm{M}})(c_{\mathrm{A}}+c_{\mathrm{M}})(l_{\mathrm{A}}-\zeta)T}{\mu(l_{\mathrm{A}}-\zeta)(2c_{\mathrm{T}}+c_{\mathrm{A}}-c_{\mathrm{M}})\sinh\left(\mu\frac{\zeta}{2}\right)\cosh(\mu\xi_0)+(c_{\mathrm{A}}+c_{\mathrm{M}})\left[\cosh\left(\mu\frac{\zeta}{2}\right)\cosh(\mu\xi_0)-\sinh\left(\mu\frac{\zeta}{2}\right)\sinh(\mu\xi_0)\right]-\mu(l_{\mathrm{A}}-\zeta)(c_{\mathrm{A}}+c_{\mathrm{M}})\cosh\left(\mu\frac{\zeta}{2}\right)\sinh(\mu\xi_0)}$$

(18)

Eq. 17 and Eq. 18 are equivalent to Eq. A6 and Eq. A7 of FHS1981 respectively.

The compliance per half sarcomere, C_{hs}, is obtained by calculating the total strain S_{hs} that an external force T induces on the half-sarcomere, and dividing the result by T, according to the relation $C_{\mathrm{hs}} = S_{\mathrm{hs}}/T$.

Going from the M line to the Z line there are four possible paths to calculate S_{hs}, and of course the results are the same.

The same path as in FHS1981 (where the possible paths are just two, since there is no titin link) is followed here. S_{hs} is given by the sum of the strain of the thick filament within the H zone (from the M line to the beginning of the overlap with the thin filament), the displacement of tip of the thin filament with respect to thick filament (or the strain of cross-bridges array at A, x_{A}), the extension of the thin filament in the overlap region, and the extension of thin filament within the I-band (Fig. 4):

$$S_{\mathrm{hs}} = c_{\mathrm{M}}(l_{\mathrm{M}} - \zeta)T + x_{\mathrm{A}} + c_{\mathrm{A}}\int_{-\frac{\zeta}{2}}^{+\frac{\zeta}{2}} T_{\mathrm{A}}(\xi)\mathrm{d}\xi + c_{\mathrm{A}}(l_{\mathrm{A}} - \zeta)\frac{c_{\mathrm{T}}}{c_{\mathrm{A}}+c_{\mathrm{T}}}\left\{T - \frac{x_{\mathrm{B}}}{c_{\mathrm{T}}(l_{\mathrm{A}}-\zeta)}\right\} \tag{19}$$

Eq. 15 is equivalent to Eq. A8 in FHS1981, and similarly, from Eq. 7:

$$T_{\mathrm{A}} = \frac{\frac{\mathrm{d}x}{\mathrm{d}\xi} + c_{\mathrm{M}}T}{c_{\mathrm{A}} + c_{\mathrm{M}}}$$

and the integral in Eq. 19 becomes:

$$\int_{-\frac{\zeta}{2}}^{+\frac{\zeta}{2}} T_{\mathrm{A}}(\xi)\mathrm{d}\xi = \frac{x_{\mathrm{B}} - x_{\mathrm{A}}}{c_{\mathrm{A}} + c_{\mathrm{M}}} + \frac{c_{\mathrm{M}}T}{c_{\mathrm{A}} + c_{\mathrm{M}}}\zeta \tag{20}$$

Thus:

$$\begin{aligned} C_{\mathrm{hs}} &= c_{\mathrm{M}}(l_{\mathrm{M}} - \zeta) + \frac{x_{\mathrm{A}}}{T} + \frac{c_{\mathrm{A}}}{c_{\mathrm{A}} + c_{\mathrm{M}}}\frac{x_{\mathrm{B}} - x_{\mathrm{A}}}{T} + \frac{c_{\mathrm{A}}c_{\mathrm{M}}}{c_{\mathrm{A}} + c_{\mathrm{M}}}\zeta + (l_{\mathrm{A}} - \zeta)\frac{c_{\mathrm{A}}c_{\mathrm{T}}}{c_{\mathrm{A}} + c_{\mathrm{T}}} - \frac{c_{\mathrm{A}}}{(c_{\mathrm{A}} + c_{\mathrm{T}})}\frac{x_{\mathrm{B}}}{T} = \\ &= c_{\mathrm{M}}(l_{\mathrm{M}} - \zeta) + \frac{c_{\mathrm{A}}c_{\mathrm{M}}}{c_{\mathrm{A}} + c_{\mathrm{M}}}\zeta + \frac{c_{\mathrm{A}}c_{\mathrm{T}}}{c_{\mathrm{A}} + c_{\mathrm{T}}}(l_{\mathrm{A}} - \zeta) + \frac{x_{\mathrm{A}}}{T} + \frac{c_{\mathrm{A}}}{c_{\mathrm{A}} + c_{\mathrm{M}}}\frac{x_{\mathrm{B}} - x_{\mathrm{A}}}{T} - \frac{c_{\mathrm{A}}}{(c_{\mathrm{A}} + c_{\mathrm{T}})}\frac{x_{\mathrm{B}}}{T} = \\ &= c_{\mathrm{M}}(l_{\mathrm{M}} - \zeta) + \frac{c_{\mathrm{A}}c_{\mathrm{M}}}{c_{\mathrm{A}} + c_{\mathrm{M}}}\zeta + \frac{c_{\mathrm{A}}c_{\mathrm{T}}}{c_{\mathrm{A}} + c_{\mathrm{T}}}(l_{\mathrm{A}} - \zeta) + \frac{x_{\mathrm{A}}}{T}\left(\frac{c_{\mathrm{M}}}{c_{\mathrm{A}} + c_{\mathrm{M}}}\right) + \frac{x_{\mathrm{B}}}{T}\left[\frac{c_{\mathrm{A}}(c_{\mathrm{T}} - c_{\mathrm{M}})}{(c_{\mathrm{A}} + c_{\mathrm{M}})(c_{\mathrm{A}} + c_{\mathrm{T}})}\right] \end{aligned} \tag{21}$$

Finally, substituting x_{A} and x_{B} with $x_0 \cosh\left(\mu\left(-\frac{\zeta}{2} - \xi_0\right)\right)$ and $x_0 \cosh\left(\mu\left(+\frac{\zeta}{2} - \xi_0\right)\right)$ respectively, and using Eq. 17 and Eq. 18 lead to:

$$\begin{aligned} &C_{\mathrm{hs}} \\ &= c_{\mathrm{M}}(l_{\mathrm{M}} - \zeta) + \frac{c_{\mathrm{A}}c_{\mathrm{T}}}{c_{\mathrm{A}} + c_{\mathrm{T}}}(l_{\mathrm{A}} - \zeta) + \frac{c_{\mathrm{A}}c_{\mathrm{M}}}{c_{\mathrm{A}} + c_{\mathrm{M}}}\zeta \\ &+ \frac{\mu\frac{{c_{\mathrm{T}}}^2}{c_{\mathrm{A}} + c_{\mathrm{T}}}(l_{\mathrm{A}} - \zeta) + 2\tanh\left(\frac{\mu\zeta}{2}\right)\frac{{c_{\mathrm{M}}}^2}{c_{\mathrm{A}} + c_{\mathrm{M}}} + \mu\tanh\left(\frac{\mu\zeta}{2}\right)^2(l_{\mathrm{A}} - \zeta)\frac{[c_{\mathrm{T}}(c_{\mathrm{M}} - c_{\mathrm{A}}) + 2c_{\mathrm{A}}c_{\mathrm{M}}]^2}{(c_{\mathrm{M}} + c_{\mathrm{A}})^2(c_{\mathrm{T}} + c_{\mathrm{A}})}}{\mu\left[1 + 2\mu\tanh\left(\frac{\mu\zeta}{2}\right)\frac{c_{\mathrm{A}} + c_{\mathrm{T}}}{c_{\mathrm{A}} + c_{\mathrm{M}}}(l_{\mathrm{A}} - \zeta) + \tanh\left(\frac{\mu\zeta}{2}\right)^2\right]} \end{aligned}$$

(22)

Provided that $\mu\zeta/2$ is not too large, dividing both numerator and denominator of the last term for $\tanh(\mu\zeta/2)$ and using the approximations:

$$\tanh\left(\frac{\mu\zeta}{2}\right) \approx \frac{\mu\zeta}{2}$$

and

$$\coth\left(\frac{\mu\zeta}{2}\right) \approx \frac{2}{\mu\zeta} + \frac{1}{3}\frac{\mu\zeta}{2}$$

Eq. 22 can be approximated by:

$$C_{\mathrm{hs}} = c_{\mathrm{M}}(l_{\mathrm{M}} - \zeta) + \frac{c_{\mathrm{A}} c_{\mathrm{T}}}{c_{\mathrm{A}} + c_{\mathrm{T}}}(l_{\mathrm{A}} - \zeta) + \frac{c_{\mathrm{A}} c_{\mathrm{M}}}{c_{\mathrm{A}} + c_{\mathrm{M}}}\zeta + \frac{\frac{{c_{\mathrm{T}}}^2}{c_{\mathrm{A}} + c_{\mathrm{T}}}(l_{\mathrm{A}} - \zeta) + \frac{{c_{\mathrm{M}}}^2}{c_{\mathrm{A}} + c_{\mathrm{M}}}\zeta + \frac{k_{\mathrm{c}}\zeta^2(l_{\mathrm{A}} - \zeta)}{12(c_{\mathrm{A}} + c_{\mathrm{T}})}\left\{{c_{\mathrm{T}}}^2(c_{\mathrm{M}} + c_{\mathrm{A}}) + \frac{3[c_{\mathrm{T}}(c_{\mathrm{M}} - c_{\mathrm{A}}) + 2c_{\mathrm{A}}c_{\mathrm{M}}]^2}{c_{\mathrm{M}} + c_{\mathrm{A}}}\right\}}{1 + \frac{k_{\mathrm{c}}\zeta}{3}[\zeta(c_{\mathrm{A}} + c_{\mathrm{M}}) + 3(l_{\mathrm{A}} - \zeta)(c_{\mathrm{A}} + c_{\mathrm{T}})]}$$

(23)

where the dependence of C_{hs} on k_{c}, the stiffness per unit length of the motor array, is made explicit.

RESULTS

When $c_{\mathrm{T}} \to \infty$, Eq. 22 and Eq. 23 reduce to Eq. A9 and Eq. A10 of FHS1981, as expected. On the contrary, when k_{c}, and then μ, → 0 or $c_{\mathrm{A}} \to \infty$, while FHS1981 predicts $C_{\mathrm{hs}} \to \infty$, Eq. 22 predicts $C_{\mathrm{hs}} = c_{\mathrm{M}} l_{\mathrm{M}} + c_{\mathrm{T}}(l_{\mathrm{A}} - \zeta)$, i.e. the series of thick filament and I-band titin compliances. These results are consistent with the structural/mechanical models drawn in Fig. 2 and Fig. 4 respectively.

The main difference introduced by the I-band spring that links the edge of the thick filament to the Z line is that in this case the compliance of the half-sarcomere cannot any longer be thought as the sum of compliances in series, even within the approximation that leads to Eq. A10 of FHS1981. Thus, while FHS1981 allowed to define an equivalent filament compliance C_{f} contributing to C_{hs}, as represented by Eq. 3, when the contribution of titin is considered, the concept of equivalent filament compliance is no longer applicable.

Experimentally, the values of the parameters c_{A}, c_{M}, c_{T}, k_{c} can be estimated, for example, by applying fast (4 kHz) length oscillations to a muscle fiber during the rise of an isometric tetanus (11) to measure C_{hs} at several force levels during the rise of an isometric tetanus. The number of attached motors (n_{A}) varies linearly with force (37), and so does their stiffness: $k_{\mathrm{c}}\zeta = k_{\mathrm{c0}}\zeta T$, where k_{c0} is the stiffness per unit length of the cross-bridge array at the maximal isometric force T_0, and T is the force during the tetanus rise expressed in T_0 units. In this way, the values of C_{hs} at different T can be fitted by Eq. 22 or Eq. 23 to determine the different parameters.

As an example, to evaluate the possible contribution of titin to the half-sarcomere compliance, we have calculated how C_{hs} from Eq. 22 should vary during the tetanus rise with the values for c_{A}, c_{M} and k_{c0} as estimated in (38), and with different values for c_{T}. Here we neglect the possible contribution of the compliance in parallel with the cross-bridges (C_{p}). In (38) the values of the myofilament compliances are estimated by means of X-ray diffraction measurements as c_{A} = 2.29 nm/T_0/μm and c_{M} = 2.80 nm/T_0/μm, and, by comparing these results with mechanical measurements, k_{c0} is calculated to be 0.806 T_0/nm/μm. The results are reported in Fig. 4, where C_{hs} as a function of T is plotted for different c_{T} (1, 10, 100 and 1000 nm/T_0/μm) at four different sarcomere lengths (SL), 2.15 (A), 2.5 (B), 2.7 (C) and 2.90 μm (D) (and correspondingly different ζ from 0.7 to 0.325 μm, having taken l_{A}=0.975 μm and l_{M}=0.8 (38)). It can be seen that the presence of a titin-like compliance with c_{T} of 10 nm/T_0/μm or less (short-dashed lines) is not compatible with the observed C_{hs}-T relation at 2.15 μm (11), as in this case, unlike what observed, C_{hs} at lower forces is systematically reduced with respect to the value in the absence of the titin-like spring to a value that is almost constant independent of isometric force, which is directly proportional to n_{A}. Instead for higher c_{T} values (100 nm/T_0/μm or larger, long-dashed lines), C_{hs} at high forces (or n_{A}) is unaffected, while at low forces it is reduced by an extent that is larger at smaller forces in agreement with experimental results at 2.15 um SL (11) and, at any force, is larger at longer SL.

Superimposed C_{hs}-force relations at the four SL are shown in Fig. 5 in the absence of a titin-like spring (A, B) and with a titin-like spring with c_T 100 nm/T_0/µm (C, D). In the expanded scale it can be seen that in the absence of titin (B) the increase in C_{hs} with SL (that is with the reduction of filament overlap) present at high forces becomes progressively smaller with the reduction of force, since C_{hs} tends to ∞ as n_A tends to zero. Instead, in the presence of a titin-like spring with c_T 100 nm/T_0/µm, the SL-dependent upward shift in C_{hs} remains at any force, as at low force the contribution of titin takes over that of n_A.

DISCUSSION

The contribution to the compliance of a titin-like I-band spring emerges whenever, like at low level of force during the rise of an isometric tetanus, the number of attached motors n_A is relatively small with respect to those attached at the isometric tetanus plateau. In this way the I-band spring prevents C_{hs} to rise to infinite as n_A approaches zero (Fig. 6). The reduction of Chs is larger if the compliance of the titin-like element (c_T) is smaller and, for a given value of c_T, is larger at lower forces. This is emphasised in Fig. 7A, where the points (extracted by the relations in Fig. 6) indicate the relation between C_{hs} and c_T at 0.5 T_0 (triangles) and 0.1 T_0 (circles). The reduction in C_{hs} produced by introducing a titin-like spring with a c_T of 100 nm/T_0/µm is estimated at 0.1 T_0 and at 0.5 T_0 by the length of the segment *m* and *n* respectively, showing that the effect of titin is 12 times larger at 0.1 than at 0.5 T_0. In this respect the contribution of an I-band spring like titin is similar to that of an A-band spring as that represented by a fraction of no-force generating or weakly-bound motors in parallel with the array of force generating motors (10,12).

The effect on C_{hs} of an I-band spring like titin with respect to that of an A-band spring may become quite more specific in relation to changes in sarcomere length. The question is analysed in Fig. 7B by comparing the relations between C_{hs} and SL at force 0.1 T_0, at which both an I-band and an A-band spring produce a large effect, obtained either with the contribution of cross-bridges in the absence of any added spring (circles) or in the presence of either an A-band spring like that determined in (11) (squares, C_p = 29 nm/T_0) or an I-band spring with c_T of 100 nm/T_0/µm (triangles), 50 nm/T_0/µm (reverse triangles) and 10 nm/T_0/µm (diamonds). At SL 2.15 µm an A-band spring with C_p 29 nm/T_0 decreases C_{hs} by almost the same amount (~35%) as an I-band spring with c_T 100 nm/T_0/µm. In fact, taking into account the length of the I-band spring (SL/2 – l_M = 0.275 µm), the actual I-band spring compliance C_T is (100 nm/T_0/µm·0.275 µm =) 27 nm/T_0, not significantly different from C_p of the A-band spring determined in (11) at SL 2.15 µm (square). Thus, both the I-band and the A-band springs with constant stiffness do contribute to increase C_{hs} with the increase in SL, as demonstrated by the finding that the slopes of both C_{hs}-SL relations identified by squares and triangles are larger than the slope of the C_{hs} – SL relation calculated with the contribution of cross-bridges without any added spring (circles). The C_{hs}-SL relation is shifted progressively downward with the reduction of c_T to 50 nm/T_0/µm (reverse triangles) and 10 nm/T_0/µm (diamonds).

It must be noted that the relations in Fig. 7B represent the theoretical predictions of the effect on C_{hs} of springs that have a constant compliance per unit length. To apply these predictions to the contribution to C_{hs} of a titin-like I-band spring in situ, we may need to take into account of experimental evidence (first of all the passive force-SL relation, but also the response of active muscle to sudden larger stretch (31)) showing that titin stiffness increases at larger SL. Actually, yet neither in situ nor in vitro measurements of SL dependence of titin stiffness have been performed with small length perturbation in the ≥ 4kHz frequency domain, which should prevent the confounding effects of the faster components of the relaxation processes related to titin unfolding (27,39) and motor detachment/attachment (40). It looks likely, anyway, that also in the active

muscle, as in the resting muscle, titin stiffness increases with SL. Under these conditions the relations in Fig. 7B provide a fundamental tool to interpret the changes in C_{hs} related to the contribution of a titin-like I-band spring. As an example, let's assume that c_T at SL 2.15 µm is 100 nm/T_0/µm and compare the C_{hs} attained at SL 2. 7 µm with c_T 100 nm/T_0/µm (triangle) to that with c_T 50 nm/T_0/µm (reverse triangle). If c_T does not change with the increase in SL, C_{hs} at 2.7 µm (triangle) increases by 25%, as the result of both the reduction of n_A (due to the reduction of filament overlap by 0.25 nm) and doubling of the length of the I-band spring, (SL/2 – l_M), from 0.275 to 0.55 µm. However, if we assume that titin is a tunable spring which perfectly adapts its stiffness to the large changes in the I-band length, so that its c_T is halved when its length is doubled, then by increasing the SL from 2.15 to 2.7 µm (which doubles the I-band spring length) the change in C_{hs} would be quite smaller as it would depend only on the reduction in number of attached motors with reduction in overlap, as shown by comparing the ordinate value of the filled triangle (c_T 100 nm/T_0/µm, SL 2.15 µm) with the filled reverse triangle (c_T 50 nm/T_0/µm, SL 2.7 µm).

AUTHOR CONTRIBUTIONS

M.R. developed the mathematical formalism. I.P. made the numerical calculations. M.C. and M.R. wrote the manuscript.

ACKNOWLEDGMENT

We thank Vincenzo Lombardi for insightful comments on the manuscript. This work was supported by University of Florence (competitive project rictd1819) (Italy).

REFERENCES

1. Huxley, A. F., and R. M. Simmons. 1971. Proposed mechanism of force generation in striated muscle. Nature 233:533-538.

2. Ford, L. E., A.F. Huxley, and R. M. Simmons. 1977. Tension responses to sudden length change in stimulated frog muscle fibres near slack length. J. Physiol. 269:441-515.

3. Huxley, H.E , A. Stewart, H. Sosa, and T. Irving. 1994. X-ray diffraction measurements of the extensibility of actin and myosin filaments in contracting muscle. Biophys. J. 67:2411-2421.

4. Huxley, H.E., M. Reconditi, A. Stewart, and T. Irving. 2006. X-ray interference studies of crossbridge action in muscle contraction: evidence from quick releases. J. Mol. Biol. 363:743-761.

5. Wakabayashi, K., Y. Sugimoto, H. Tanaka, Y. Ueno, Y. Takezawa, and Y.Amemiya. 1994. X-ray diffraction evidence for the extensibility of actin and myosin filaments during muscle contraction. Biophys. J. 67:2422-2435.

6. Reconditi, M., M. Linari, L. Lucii, A. Stewart, Y.-B. Sun, P. Boesecke, T. Narayanan, R. F. Fischetti, T. Irving, G. Piazzesi, M. Irving, and V. Lombardi. 2004. The myosin motor in muscle generates a smaller and slower working stroke at higher load. Nature 428:578-581.

7. Piazzesi, G., M. Reconditi, M. Linari, L. Lucii, P. Bianco, E. Brunello, V. Decostre, A. Stewart, D. B. Gore, T. C. Irving, M. Irving, and V. Lombardi. 2007. Skeletal muscle performance determined by modulation of number of myosin motors rather than motor force or stroke size. Cell 131:784-795.

8. Ford, L. E., A. F. Huxley, and R. M. Simmons. 1981. The relation between stiffness and filament overlap in stimulated frog muscle fibres. J. Physiol. 311:219-249.

9. Fusi, L., M. Reconditi, M. Linari, E. Brunello, R. Elangovan, V. Lombardi, and G. Piazzesi. 2010. The mechanism of the resistance to stretch of isometrically contracting single muscle fibres. J. Physiol. 588:495-510.

10. Colombini, B., M. Nocella, M. A. Bagni, P. J. Griffiths, and G. Cecchi. 2010. Is the cross-bridge stiffness proportional to tension during muscle fiber activation? Biophys. J. 98:2582-2590.

11. Fusi, L., E. Brunello, M. Reconditi, G. Piazzesi, and V. Lombardi. 2014. The non-linear elasticity of the muscle sarcomere and the compliance of myosin motors. J. Physiol. 592:1109-1118.

12. Fusi, L., V. Percario, E. Brunello, M. Caremani, P. Bianco, J. D. Powers, M. Reconditi, V. Lombardi, and G. Piazzesi. 2017. Minimum number of myosin motors accounting for shortening velocity under zero load in skeletal muscle. J. Physiol. 595:1127-1142.

13. Offer, G., C. Moos, and R. Starr. 1973. A new protein of the thick filaments of vertebrate skeletal myofibrils. Extractions, purification and characterization. J. Mol. Biol. 74:653-676

14. Moos, C. 1981. Fluorescence microscope study of the binding of added C protein to skeletal muscle myofibrils. J. Cell. Biol. 90:25–31.

15. Yamamoto, K. 1986. The binding of skeletal muscle C-protein to regulated actin. FEBS Lett. 208:123–127.

16. Squire, J. M., M. Roessle, and C. Knupp. 2004. New X-ray diffraction observations on vertebrate muscle: organisation of C-protein (MyBP-C) and troponin and evidence for unknown structures in the vertebrate A-band. J. Mol. Biol. 343:1345-1363.

17. Luther, P. K., H. Winkler, K. Taylor, M. E. Zoghbi, R. Craig, R. Padrón, J. M. Squire, and J. Liu. 2011. Direct visualization of myosin-binding protein C bridging myosin and actin filaments in intact muscle. Proc. Natl. Acad. Sci. U. S. A. 108:11423–11428.

18. Rybakova, I. N., M. L. Greaser, and R. L. Moss. 2011. Myosin binding protein C interaction with actin: characterization and mapping of the binding site. J. Biol. Chem. 286:2008-2016.

19. Pfuhl, M., and M. Gautel. 2012. Structure, interactions and function of the N-terminus of cardiac myosin binding protein C (MyBP-C): who does what, with what, and to whom? J. Muscle Res. Cell. Motil. 33:83–94.

20. Maruyama, K., S. Matsubara, R. Natori, Y. Nonomura, and S. Kimura. 1977. Connectin, an elastic protein of muscle. Characterization and Function. J. Biochem. 82:317-337.

21. Wang, K., J. McClure, and A. Tu. 1979. Titin: major myofibrillar components of striated muscle. Proc. Natl. Acad. Sci. U. S. A. 76:3698–3702.

22. Fürst, D. O., M. Osborn, R. Nave, and K. Weber. 1988. The organization of titin filaments in the half-sarcomere revealed by monoclonal antibodies in immunoelectron microscopy: a map of ten nonrepetitive epitopes starting at the Z line extends close to the M line. J. Cell. Biol. 106:1563-1572.

23. Linke, W. A., M. Kulke, H. Li, S. Fujita-Becker, C. Neagoe, D. J. Manstein, M. Gautel and J. M. Fernandez. 2002. PEVK domain of titin: an entropic spring with actin-binding properties. J Struct. Biol. 137:194-205.

24. Granzier, H.L., and S. Labeit. 2004. The giant protein titin: a major player in myocardial mechanics, signaling, and disease. Circ Res. 94:284-295.

25. Reconditi, M., E. Brunello, L. Fusi, M. Linari, M. F. Martinez, V. Lombardi, M. Irving, and G. Piazzesi. 2014. Sarcomere-length dependence of myosin filament structure in skeletal muscle fibres of the frog. J. Physiol. 592:1119–1137.

26. Powers, J.D, M. Reconditi, L. Fusi, E. Brunello, V. Lombardi, and G. Piazzesi. 2017. Evidence for an I-Band Spring that is Tuned to the Length of the Skeletal Muscle Sarcomere. Biophys. J. 112:p181a.

27. Rivas-Pardo, J. A., E. C. Eckels, I. Popa, P. Kosuri, W. A. Linke, and J. M. Fernández. 2016. Work done by titin protein folding assists muscle contraction. Cell Reports 14:1339-1347.

28. Rassier, D.E., E.-J. Lee, and W. Herzog. 2005. Modulation of passive force in single skeletal muscle fibres. Biol. Lett. 1:342-345.

29. Rassier, D.E., F.S. Leite, M. Nocella, A.S. Cornachione, B. Colombini, and M.A. Bagni. 2015. Non-crossbridge forces in activated striated muscles: a titin dependent mechanism of regulation? J. Muscle Res. Cell Motil. 36:37-45.

30. A.S. Cornachione, F. Leite, M.A. Bagni, and D.E. Rassier. 2016. The increase in non-cross-bridge forces after stretch of activated striated muscle is related to titin isoforms. Am. J. Physiol. Cell Physiol. 310:C19-C26

31. Bagni, M. A., G. Cecchi, B. Colombini, and F. Colomo. 2002. A non-cross-bridge stiffness in activated frog muscle fibers. Biophys. J. 82:3118-3127.

32. Labeit, D., K. Watanabe, C. Witt, H. Fujita, Y. Wu, S. Lahmers, T. Funck, S. Labeit, and H. Granzier. 2003. Calcium-dependent molecular spring elements in the giant protein titin. Proc. Natl. Acad. Sci. U. S. A. 100:13716-13721.

33. Linari, M., E. Brunello, M. Reconditi, L. Fusi, M. Caremani, T. Narayanan, G. Piazzesi, V. Lombardi, and M. Irving. 2015. Force generation by skeletal muscle is controlled by mechanosensing in myosin filaments. Nature 528:276–279.

34. Reconditi, M., M. Caremani, F. Pinzauti, J. D. Powers, T. Narayanan, G. J. M. Stienen, M. Linari, V. Lombardi, and G. Piazzesi. 2017. Myosin filament activation in the heart is tuned to the mechanical task. Proc. Natl. Acad. Sci. U. S. A. 114:3240-3245.

35. Piazzesi, G., M. Caremani, M. Linari, M. Reconditi, and V. Lombardi. 2018 Thick filament mechano-sensing in skeletal and cardiac muscles: a common mechanism able to adapt the energetic cost of the contraction to the task. Front. Physiol. 9:736

36. Luther, P. K. 2009. The vertebrate muscle Z-disc: sarcomere anchor for structure and signalling. J. Muscle Res. Cell. Motil.30:171-185

37. Brunello, E., P. Bianco, G. Piazzesi, M. Linari, M. Reconditi, P. Panine, T. Narayanan, W. I. Helsby, M. Irving, and V. Lombardi. 2006. Structural changes in the myosin filament and cross-bridges during active force development in single intact frog muscle fibres: stiffness and X-ray diffraction measurements. J. Physiol. 577:971-984.

38. Brunello, E., M. Caremani, L. Melli, M. Linari, M. Fernandez-Martinez, T. Narayanan, M. Irving, G. Piazzesi, V. Lombardi, and M. Reconditi. 2014. The contributions of filaments and cross-bridges to sarcomere compliance in skeletal muscle. J. Physiol. 592:3881-3899.

39. Kellermayer, M. S., S. B. Smith, H. L. Granzier, and C. Bustamante. 1997. Folding-unfolding transitions in single titin molecules characterized with laser tweezers. Science 276:1112–1116.

40. Lombardi, V., and G. Piazzesi. 1990. The contractile response during steady lengthening of stimulated frog muscle fibres. J. Physiol. 431:141-71

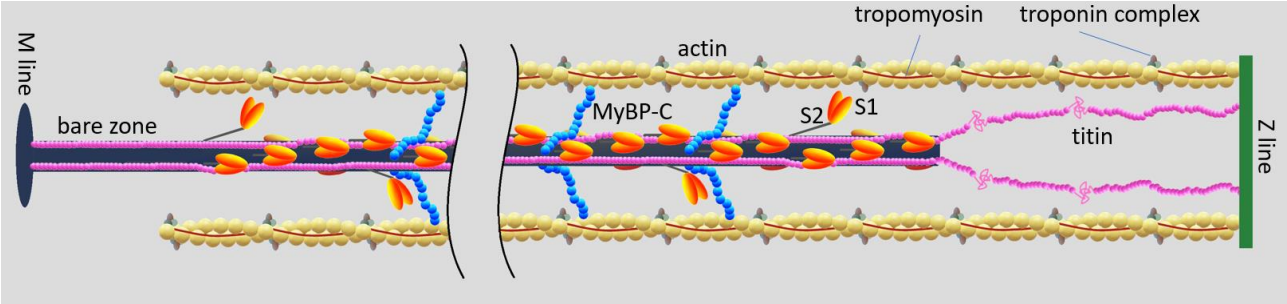

Fig. 1. Schematic representation of the half-sarcomere protein assembly. On the thin filament (yellow, formed by the actin monomer polymerization in a double helix with a period of 73 nm) are shown the regulatory proteins tropomyosin (red) and troponin complex (light and dark gray and brown). On the thick filament (dark blue) the S1 globular head domains of myosin (orange) emerge with a three stranded helical symmetry with 43 nm periodicity. The Myosin Binding Protein C (MyBP-C, blue) lies on the proximal 1/3 of the thick filament with the C-terminus and extends to thin filament with the N-terminus. Titin (pink) in the I-band connects the Z line at the end of the sarcomere (green) to the tip of the thick filament and in the A-band runs on the surface of the thick filament up to the M-line at the centre of the sarcomere. To see this figure in color, go online.

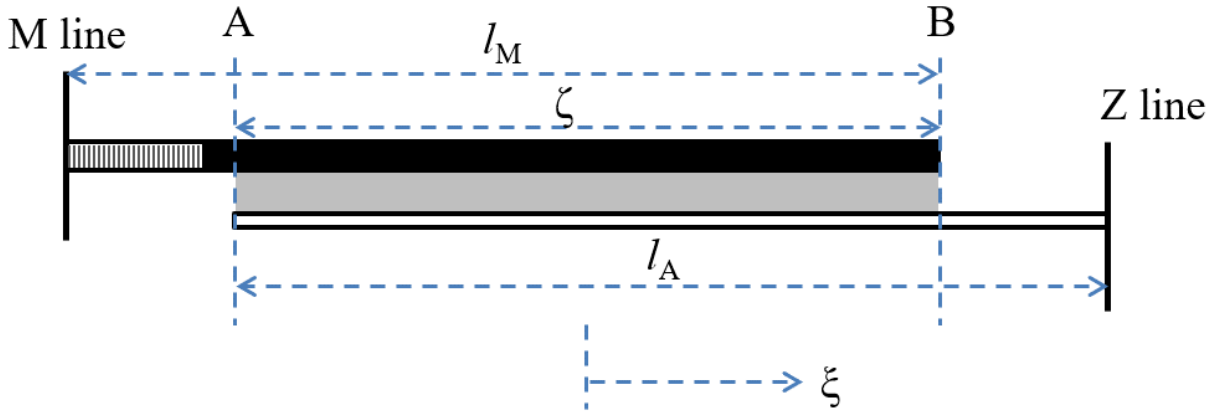

Fig. 2. Diagram indicating the arrangement of the thick and thin filaments and the cross-bridges in the half-sarcomere. The half-thick filament (length l_M; black, where myosin motors are present; dashed, bare zone, where no myosin motors are present) extends from the M line, at the center of the sarcomere. The grey band represents the cross-bridges in the region (length ζ) that overlaps with the thin filament (white; length l_A) that extends from the Z line. Motors attaching to the thin filament (cross-bridges) contribute to the compliance of the half-sarcomere. ξ is the axial coordinate, with the origin in the middle of the overlap region (adapted from (8)).

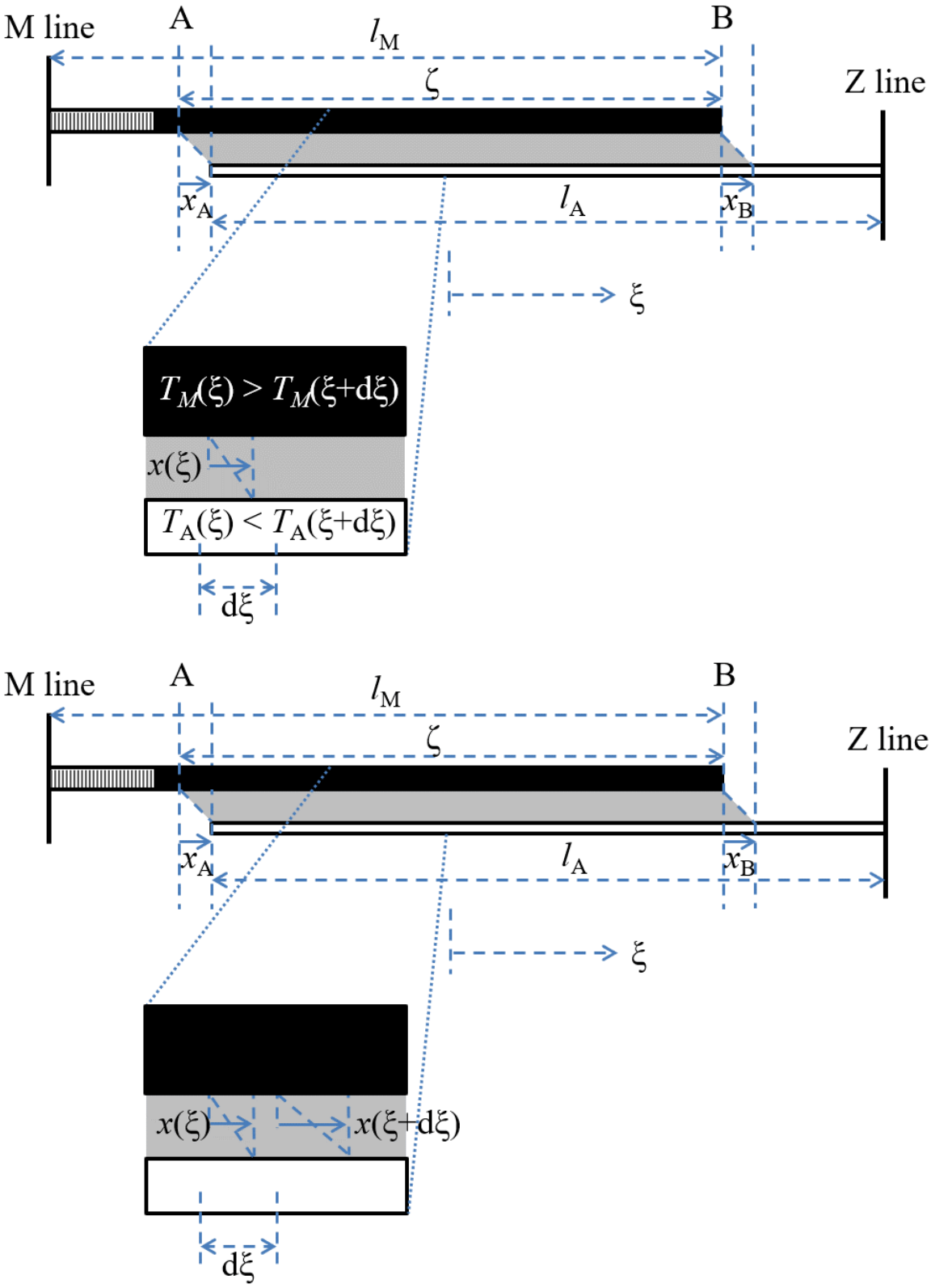

Fig. 3. Schematic of the half sarcomere strained by an external force T. x_A and x_B are the cross-bridge distortion at the point A and B along the half-sarcomeres, at coordinate $\xi = -\zeta/2$ and $\xi = +\zeta/2$ respectively. Upper panel: the expanded region around the generic coordinate ξ shows that the force in a small region $d\xi$ is transmitted between the thick and thin filament through a distortion $x(\xi)$ of the cross-bridge array segment $d\xi$ wide and $k_c d\xi$ stiff. Lower panel: in the expanded region is now indicated the different distortion x of the cross-bridge array over a small axial distance $d\xi$.

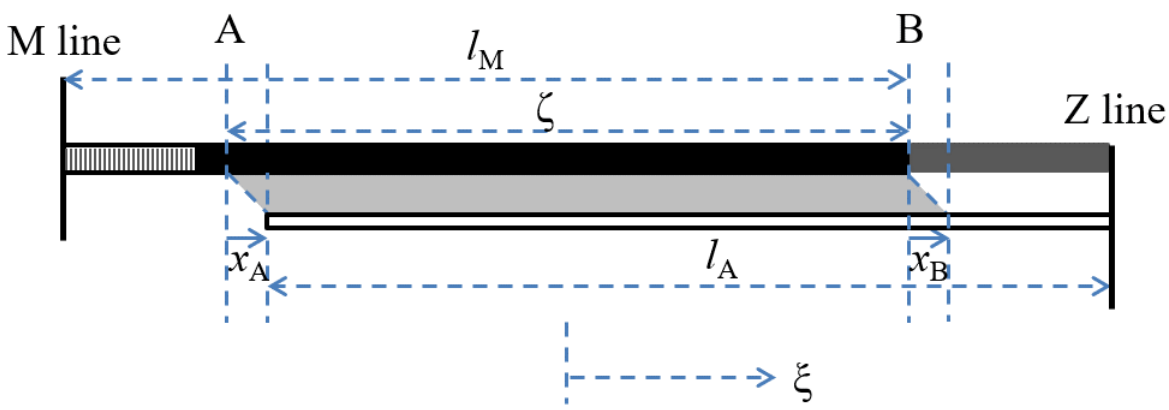

Fig. 4. Diagram of the half-sarcomere incorporating the titin (dark gray band, extending from the Z line to the edge of the thick filament). When an axial force is applied to the half-sarcomere, the strain of the titin is equal to the strain of the thin filament in the I band plus the strain of the cross-bridge array at B, x_B.

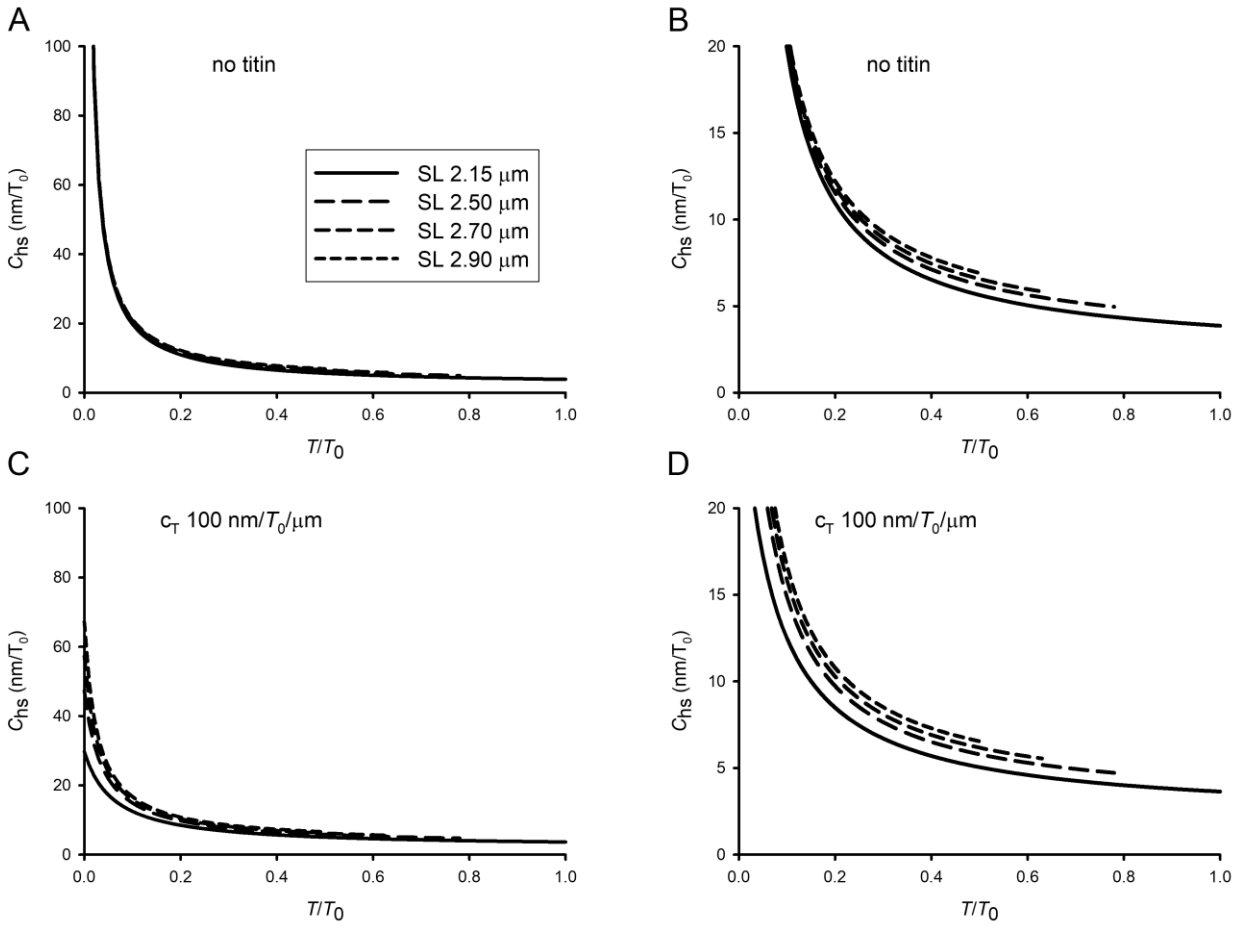

Fig. 5. Compliance of the half-sarcomere C_{hs} calculated as a function of force T during the rise of an isometric tetanus at different sarcomere lengths (SL, as in the inset) in the absence (A, B) or in the presence (C, D) of titin with a compliance per unit length c_T = 100 nm/T_0/μm.

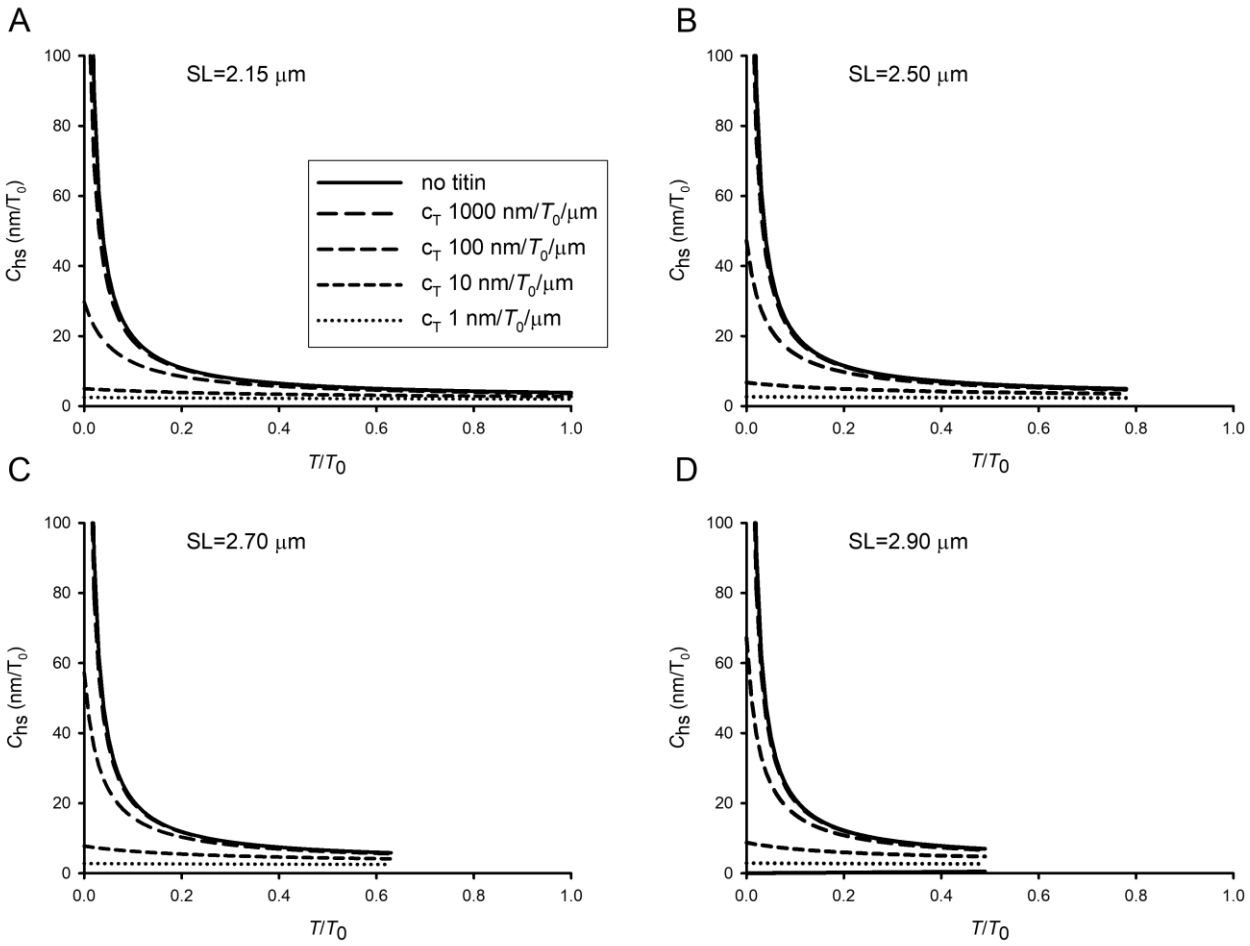

Fig. 6. Compliance of the half sarcomere C_{hs} calculated as a function of force T during the rise of an isometric tetanus for different values of titin compliance per unit length (c_T, as in the inset) and at four different sarcomere lengths (A. SL = 2.15 µm; B. SL = 2.50 µm; C. SL = 2.70 µm; D. SL = 2.90 µm). T_0 is the maximal tetanic force developed in isometric contraction at SL = 2.15 µm. c_A, c_M and k_c from Brunello et al 2014 (see text). l_A = 0.975 µm, l_M = 0.8 µm.

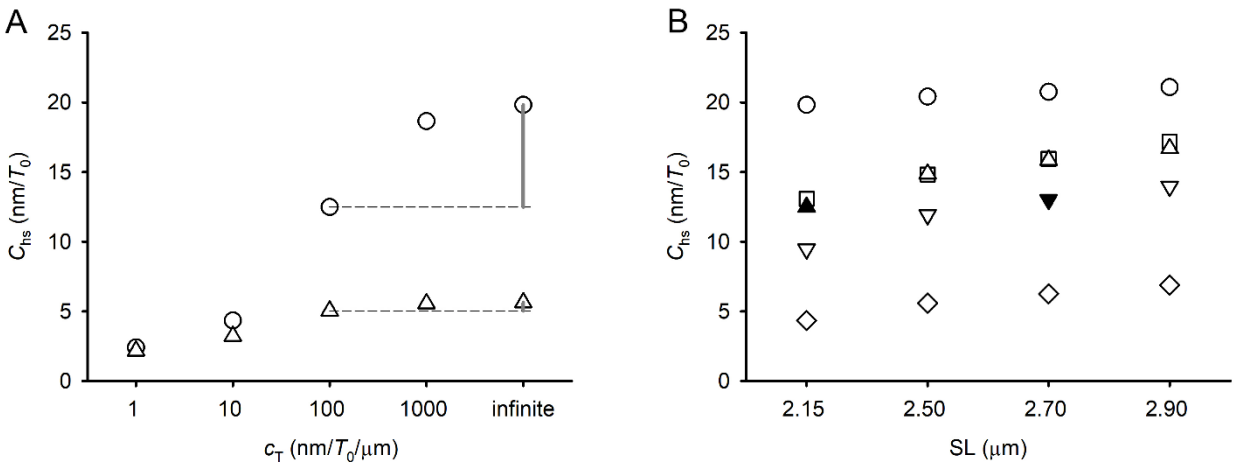

Fig. 7. A. Compliance of the half-sarcomere C_{hs} calculated as a function of titin compliance per unit length, c_T, at SL 2.15 μm at forces 0.1 T_0 (circles) and 0.5 T_0 (triangles) during the rise of an isometric tetanus. The vertical gray lines indicate the reduction in C_{hs} caused by introducing an I-band spring with c_T = 100 nm/T_0/μm at either 0.1 T_0 (m) or 0.5 T_0 (n). B. Compliance of the half-sarcomere C_{hs} calculated as a function of SL at 0.1 T_0. Circles: C_{hs} contributed only by the myofilaments and cross-bridges; squares: effect of a parallel elastic element with compliance C_p as described in the text; triangles, reverse triangles and diamonds: effect of titin-like I-band spring with compliance c_T = 100 nm/T_0/μm, 50 nm/T_0/μm and 10 nm/T_0/μm respectively. See text for filled symbols.